Application of a Nuclear Reactor Monitoring System

Manuel Silva
University of Wisconsin-Madison, Department of Physics
(Dated: April 29, 2019)

Monitoring of nuclear reactors has many uses in the fields of nuclear and particle physics. Since the usage of this monitoring system varies widely, the distance of the detector from the source is considered an independent variable. Due to the constant bombardment of cosmic ray showers, the detector will need to be placed underground using the ground as a shield. These studies show proposed locations of nuclear reactor monitoring sites as function of the distance and depth away from the source. A selected nuclear reactor site, R. E. Ginna Nuclear Power Plant, is considered as baseline to extract the estimated fluxes. The material that the particles will transverse is granite stone and assumed to be homogeneous. The code is included that can easily be modified to accommodate different reactor cores, different detector properties, and material for cosmic ray propagation.

INTRODUCTION

One practical application of nuclear reactor monitoring is for use in nuclear and particle physics experiments that attempt to detect particles emitted from the core the nuclear reactors, mainly interested in the electron anti-neutrinos. A second, but less practical purpose (depends on who you talk to), is for the confirmation of depletion or lack of operation of an active or decommissioned nuclear reactor. These serve for national security monitoring or for validation of the power generated by these reactors with respect to the size of the source (eg safety reasons). The purpose of the nuclear reactor monitoring system (detector) drives the precise technology and location, where the cores are located and how easy it is to build a mine to place the detector as certain distances. The technology for detection of neutrinos will rely on the inverse beta decay process and will require a large target material to maximize the probability of the anti-neutrino interacting, similar techniques first employed by Cowan and Reines in the 1950s [1]. Section will outline the basic structure of the physics processes that occur within a nuclear reactor. It will also cover the basic process in which a properly constructed detector can observe such a signal. Section will go into the necessary properties of such a detector. The placement of the detector is driven by environmental aspects as well as the interpretation of such a measurement. In the case of Daya Bay [2], the precise location of the detector is necessary for detection of rare nuclear processes (neutrino oscillation). If this were not the case, then one would attempt to place the detector closer to the source to maximize the effective flux. Due to the constant bombardment of cosmic ray muons, one would need to place the detector underground to minimize the risk of misinterpreting a signal. The modeling of this reducible background is described in section . One would also need to consider irreducible backgrounds which are mainly from atmospheric neutrinos and solar neutrinos, these are described in section and . Putting all the details together, one could make a simple parametric function of the depth of such a detector as a function of the distance. The depth chosen would be the minimum depth to place the detector such that the signal can easily be observed. The threshold for a significant signal is describe in detail under the detector section. The results and optimized locations of such detectors are shown in section .

PHYSICS

Physics Background

The primary radioactive element inside a nuclear reactor core is Uranium-235. This element has a half life of 700 million years, therefore a large sample is needed to trigger the first reaction[5]. The first decay is through an alpha particle emission with a recoiled Thorium-231. The alpha particle has enough kinetic energy to trigger the fission of another U-235 atom which will produce another alpha particle to continue the process, this will continue indefinitely until the source of alpha particles is extinguished. During this process, the byproducts of fission will be highly unstable and will most likely undergo their own decays. The most probably process is Thorium-231 beta decay to Palladium-232, this beta decay produces an electron and electron anti-neutrino.

$$Th^{231} \rightarrow Pa^{232} + e^{-} + \bar{\nu}^{e} \tag{1}$$

A stable equilibrium is reached inside the reactor core since the core is normally cooled (from energy extraction) and replenishing the source. Due to the small neutrino cross-section, all electron anti-neutrinos can safely escape the nuclear core. Approximately 6 anti-neutrinos are produced per fission [6] and are emitted isotropically from the source. This can be parametrized as a flux in units of $\Phi = \frac{\text{Number}(\bar{\nu})}{s*m^2}$. The electron emitted from the beta decay is of such energies that it will be absorbed with a few inches of material and therefore may not even escape the reactor. The $\bar{\nu}$'s energy depends on the angle it was produced with respect to the electron. This angle

is not important and must therefore be translated to an energy distribution only. This can easily be computed in the case of free beta decay but there are additional effects to taken into account due to the large number of neutrons inside each atom and the large number of atoms interaction among themselves.

The second important process to understand is inverse-beta decay. This process involves an incoming electron anti-neutrino scattering off a proton inside a medium. This is literally the inverse of the fundamental process illustrated in eq. 1 and now marked in eq. 2. The probability of this interaction occurring is small and needs to be computed for all neutrino energies. This is described in .

$$\bar{\nu}^e + P \rightarrow e^+ + N \tag{2}$$

Physics Application

The beta decay process be correctly modelled using quantum field theory calculations to leading order. However, the beta decay process occurs inside a large nucleus that contains several neutrons and interactions between themselves. This perturbation is critical to obtaining a precise result. The fissile material inside the nuclear reactor core is not composed of pure U-235, and this composition must also be taken into account. To simulate a robust flux of neutrinos from nuclear reactor cores, the DRAGON [16] simulation package is often used. However, for the sake of this report, I assume that the reactor core is composed of pure U-235 and that exactly six electron anti-neutrinos are emitted per fission [6]. The distribution of the electron anti-neutrinos is shown in Daya Bay's search for neutrino oscillations [2] to be similar to that of a Gaussian centered about 1.5 MeV and standard deviation of 0.5 MeV, it contains a power law tail for higher energies and cannot exceed 8.5 MeV due to energy conservation of beta decay. My generated reactor neutrinos are shown in figure 1 for the R. E. Ginna Nuclear Power Plant after converting the rate to a flux at a distance of 0.1/1/10km. The specifications of Ginna were taken from the U.s Energy Information Agency [4]. Recall that the neutrino cross section is very small, therefore it is assumed that all neutrinos emitted from the reactor core that can, will reach our detector.

The number of neutrinos expected at the detector from the reactor core are of order $10^{11}\mathrm{m}^{-2}\mathrm{s}^{-1}$. This is a very large rate of neutrinos hitting the detector. One must now take into account the probability of an interaction occurring within the detector's volume. This is described by the cross-section and is normally derived using field theory for a neutrino interacting with a nucleus. However, at these energies it can approximated with the equation

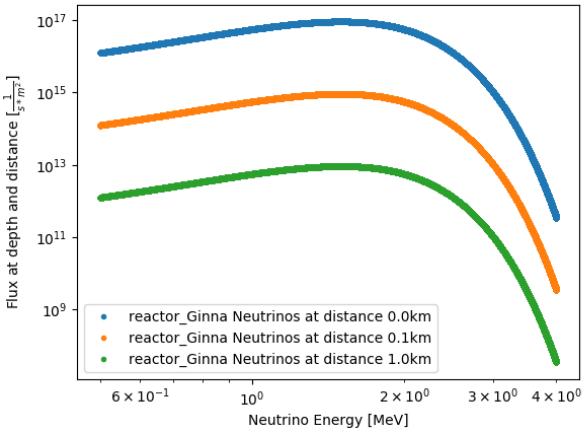

FIG. 1: The electron anti-neutrino fluxes from the reactor Ginna at several distances away from the source. The distribution of fluxes as a function of energies was that of a Gaussian and then re-weighted according to the surface area over which this flux is emitted.

$$\sigma = 6.7\mathrm{x}10^{-46}\mathrm{x}E_\nu[\mathrm{MeV}]m^2 \tag{3}$$

whereas we notice a linear dependence of the cross section with the incoming neutrino energy. Multiply the flux by the cross section will gives us the number of interactions expected per second assuming a single proton. We now take into account the size of the detector, which we talk more about in section and compute the number of total interactions occurring per second for energy.

The muons will always interact via electromagnetic forces, eg ionization. This process emits photons which will set off the sensors inside the detector. Here it is assumed that every muon that actually reach the surface of the detector will interact, this makes the calculation of the interaction probability very simple since it is merely the actual cross section of the detector. Since we assumed a $1\mathrm{m}^3$ in section , we can also take it one step further and assume a cubic volume making each dimension equal to 1m in length.

$$\sigma = \mathrm{Area}[m^2] = 1[m^2] \tag{4}$$

DETECTOR

Since the focus of this project is more about the proper identification of $\bar{\nu}$ than detector design we will chose an organic liquid scintillator material. The scintillator will provide the protons for the $\bar{\nu}$ to interact with. The positrons are assumed to interact promptly with the electrons in the medium and undergo a pair-production process of two photons. The scattered neutron is of low

energy and assumed to be captured by the nucleus. This capture will emit a second photon into the scintillator material. Using the initial photon signal from the e^+e^- interaction with a delayed second signal from the neutron capture, we can now search for $\bar{\nu}$ interactions. To simplify all calculations, the detector is assumed to be a cubic meter in size and filled with alkylbenzene, the same material used in SNO+ neutrino detector[7] and Daya Bay Reactor Neutrino Experiment [2]. The properties of this scintillator are well understood and extracted from the particle data group [5]. It will also be assumed that photomultiplier tubes (PMTs) will be placed surrounding the effective area of the detector to capture these emitted photons and measure their energies (and timing). To simplify this study, it is also assumed that the PMTs have a 100% efficiency and no error on their energy measurement.

The detector is placed underground to shield it from cosmic ray muons that may saturate the signal and prevent us from detecting a sizable flux of reactor $\bar{\nu}$. The material is assumed to be granite rock with a density of $\rho = 2.75\frac{g}{cm^3}$[8], but in future studies this value would need to be measured using the material in the hypothetical location of the detector. Once placed at a sufficiently deep site, the next biggest background would be from solar neutrinos and atmospheric neutrinos. This means that the spectrum of these processed must be correctly modeled and taken into account.

Once all reactor neutrinos and background particles are injected into our detector we must now set a standard for the quality of the signal we observe. A common benchmark number for observing a significant signal is the significance. The definition of significance is equation 5 and has been used for many optimization studies in many experiments such as LHC and TeVatron [17]. It is not know a priori if both formulas converge so both are used as a cross-check to each other. For these formulas, N_S refers to reactor neutrinos only and N_B refers to the sum of atmospheric muons and solar neutrinos. The solar neutrino background is irreducible, which implies that there will be an upper limit to the distance we can realistically place a nuclear reactor detector.

$$S = \frac{N_s}{\sqrt{N_B}}$$
$$S = \frac{N_s}{\sqrt{N_S + N_B}} \tag{5}$$

BACKGROUND MODELING

The source emits $\bar{\nu}$ in the MeV energy range. However, at these energies the detector will undergo a constant bombardment of cosmic ray byproducts. One will be the atmospheric muons and the other will be the atmospheric neutrinos. The second such background to understand is that of solar neutrinos. There will also be a small contribution from geo-neuntrinos, but the fluxes are small enough at these energy scales that they will be ignored. However, a precise measurement of neutrino properties at these energy ranges would need to properly model all these backgrounds.

Muons

Cosmic rays are constantly bombarding the Earth's atmosphere. These cosmic rays may be of extragalactic origin and some are of solar origin. These cosmic rays are extremely difficult to properly model and must therefore be taken empirically from many experiments. These cosmic rays, mostly protons at these energy scales, are shown in figure 2 taken from T. Gaisser's et al. [13].

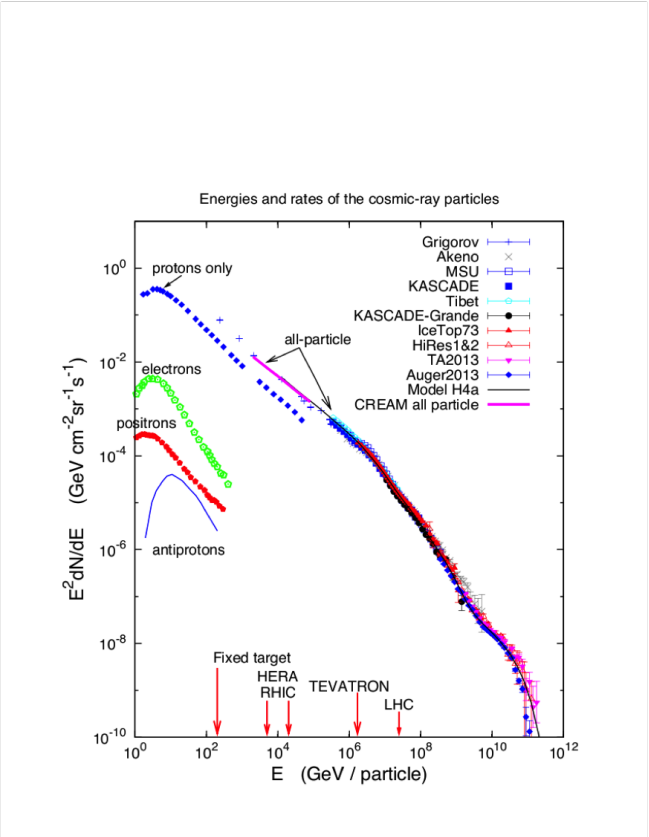

FIG. 2: The distribution of fluxes for various cosmic rays over a large energy range. For the energies we are interested in (GeV and below) there are large number of protons entering the atmosphere. These protons interact in the atmosphere and produce muons and neutrinos. Larger energy protons can also be considered but the flow is rapidly decreasing as a function of energy and therefore these higher energy protons are significantly more rare.

The cosmic rays interact in the atmosphere and produce secondary hadrons such as pions and kaons shown symbolically in eq. 6.

$$\begin{aligned} \pi^{\pm} &\rightarrow \mu^{\pm} + \nu_{\mu} \\ \mathrm{K}^{\pm} &\rightarrow \mu^{\pm} + \nu_{\mu} \end{aligned} \tag{6}$$

Muons at Sea Level

The average lifetime of muons is approximately 2.2 μs due to quantum effects. When special relativity is taken into account (due to large velocity of these muons), the muons may actually reach the Earth's surface and the detector. It is not possible to correct predict the muon flux at the Earth's surface due to the stochastic nature of cosmic ray interactions with the atmosphere. There are many variables that need to be taken into account such as the season (winter vs summer), location, and hadronic interaction models. Therefore, a full simulation of atmospheric air showers would be necessary to accurately model the muons at the Earth's surface. These computations would require an intense computational job and would require the CORSIKA package [14], however, since we are not interested in individual muon events only in the average ensemble, I use the parametrized muon flux at sea level from [15]. Table **??** contains the parameters plugged into equation 7 for muons at particular energies. We need to generate a large range of muon energies because there is a correlation with muon energy and the depth they travel until they are absorbed

$$\Phi = C * E^{-(p_1 + p_2 log(E) + p_3 log^2(E) + p_4 log^3(E))} \tag{7}$$

I sample 1000 muons for each energy ranged listed above and compute the flux for each individual muon event using the parametrization above. For each particular event, we then multiply by 4pi steradians and by the muon's energy to convert to a standardized flux of per meter squared per second. Figure 3 shows my simulation for muons at the Earth's surface.

Muons at Depth

If the detector is placed sufficiently deep underground, the muons will interact with the material and very few of them will actually reach the detector. The dominant process in which muons lose energy at MeV-GeV energies is via ionization as shown in figure 4 modeled with the Bethe-Bloch equation using granite as the material. Once the muons reach energies below 100 MeV, they begin to lose energy rapidly due to quantum effects which I will ignore. The muons in the TeV range will undergo

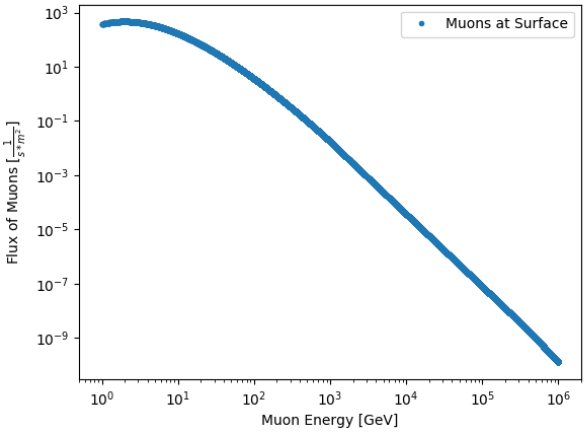

FIG. 3: My simulated muons fluxes using the parametrization of vertical muons at the Earth's surface [15]. 1 Million events were uniformly generated for each energy range, the flux was the computed for each particular muon.

energy losses due to pair production, nuclear interactions, and bremsstrahlung. These effects are all stochastic and need to computed statistically, some of these interactions are also catastrophic and the muon is converted to other particles. The flux is so low at these energy ranges, that I do not bother correctly modeling this as well.

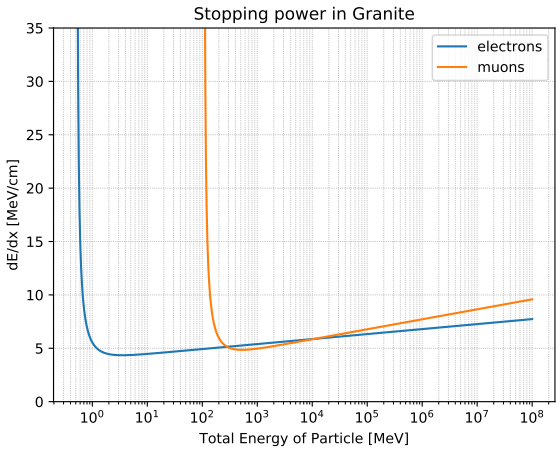

FIG. 4: Bethe-Bloch curve for muons and electrons travelling through granite rock.

Taking the muon flux at sea level and the Bethe-Bloche calculation for GeV muons, we compute the average flux at particular depths. We do this by defining a particular depth a priori and then propagating the muons to this particular depth. To better take into account the gradual change in the energy and the change in the stopping power, the muons are sampled every 10m. If the

Energy	C ($cm^{-2}s^{-1}sr^{-1}GeV^{-1}$)	p_1	p_2	p_3	p_4
1-927.7 [GeV]	2.950 x10^{-3}	0.3061	1.2743	-0.2630	0.0252
0.9277-1.588 [TeV]	1.781 x10^{-2}	1.7910	0.3040	0	0
1.588-416.2 [TeV]	1.435 x10^{1}	3.6720	0	0	0
$\geq$ 416.2 [TeV]	1 x10^{3}	4	0	0	0

TABLE I: All parameters used as input to equation 7 parametrized for vertical muons only.

muons drop below 2 MeV, the muon cannot trigger the threshold of the detector so the event is dropped. I use the stopping power from 4 along with the fluxes from 3 to compute the flux at 0.1/1/10km inside granite rock. These fluxes are shown in figure 5.

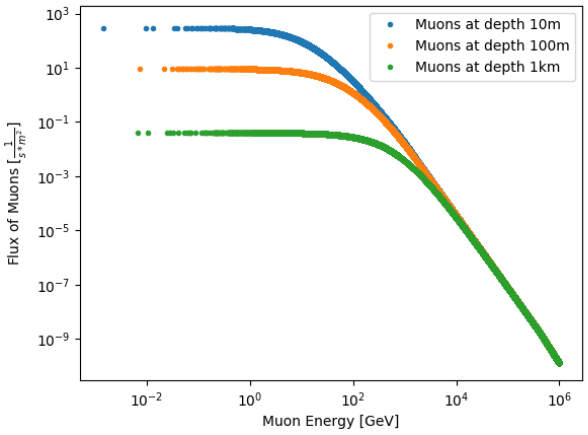

FIG. 5: The muons shown in figure 3 are propagated through the rock according to the Bethe-Bloch function. The are resampled every 10m until they reach depth. If the energy reaches 0 MeV or below, the muon is assumed to be absorbed and discarded.

Note that the energy near 1 GeV is not resolved very well, this is because the energy loss for a 1 GeV muon in granite over 10m is 5 GeV, therefore the muons is absorbed over the distance it is propagated. It is unlikely, but possible, that a sub-GeV muon will eventually reach the detector. These muons have large fluxes, therefore it is imperative that we simulate enough muons such that rare events are captured. It is also clear from figure 5 that the total flux has dropped from 10^3 to $10^{1/-1/-3}(m^{-2}s^{-1}$ for GeV muons depending on the depth. Due to ionization of muons inside the liquid scintillator, every muon that enters the detector will trigger the sensors. It is therefore imperative that the detector be built deep enough that this "noise" can be minimized.

Atmospheric Neutrinos

Atmospheric neutrinos are created when an incoming cosmic ray interacts with the atmosphere. The proton will scatter off the nitrogen in the atmosphere (most plentiful element) and produce pions and kaons along with other hadrons. These hadrons will undergo a spontaneous decay, lifetimes are of order nanoseconds, and produce muon neutrinos at a rate of 10000:1 with respect to electron neutrinos. This calculation and rate is shown in detail in Halzen and Martin [11] and the results shown in figure 8.

$$\text{Ratio} = (\frac{m_e}{m_\mu})^2(\frac{m_\pi^2 - m_e^2}{m_\pi^2 - m_\mu^2})^2 = 1.3 * 10^4 \qquad (8)$$

This means that the electron neutrinos will not be arriving from these hadronic interactions directly. Instead, the muons from these processes will undergo their own leptonic decay to a positron, an electron neutrino, and a muon anti-neutrino. Due to the complexity of these calculations I use a flux measured and parametrized from the Honda et al. group [12]. It is shown in their parametrization that the flux is about 2 orders of magnitude smaller than solar neutrino fluxes at energies lower than 20 MeV. Therefore, atmospheric neutrinos are ignored in the context of these studies. However, if one were to design a detector for neutrinos including energies more than 20 MeV, both solar and atmospheric neutrinos would need to be taken into account.

Solar Neutrinos

The solar neutrino flux is shown in fig 7 for all neutrino flavors. We are only interested in MeV neutrinos and will therefore only compute background rates for B^8 and hep processes. To take into account the number of electron neutrinos, we simply add a scaling factor of 1/3 (fraction of electron flavor neutrinos). To take into account $\bar{\nu}$ rates, we add a second scaling factor of 1/2. This means that a total effective scaling factor of 1/6 is applied to the rates in fig 7. Since the neutrinos are known to have a small cross section, interactions before reaching the detector are ignored and this flux is propagated from the surface of the Earth to depth Z.

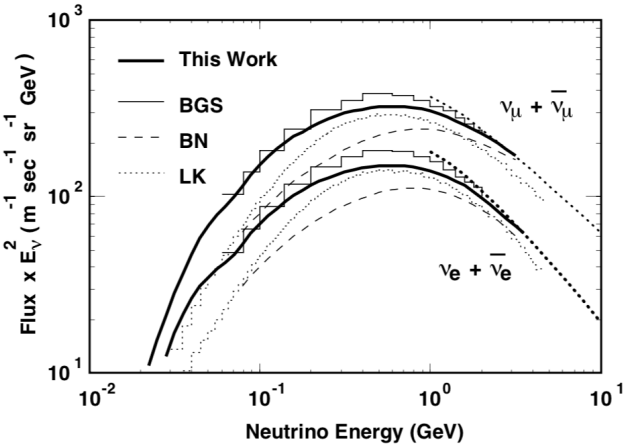

FIG. 6: Parametric atmospheric neutrino fluxes. The parametrization can be extrapolated for energies lower than 10 MeV, but the flux is already so low at these energies that this flux can be neglected.

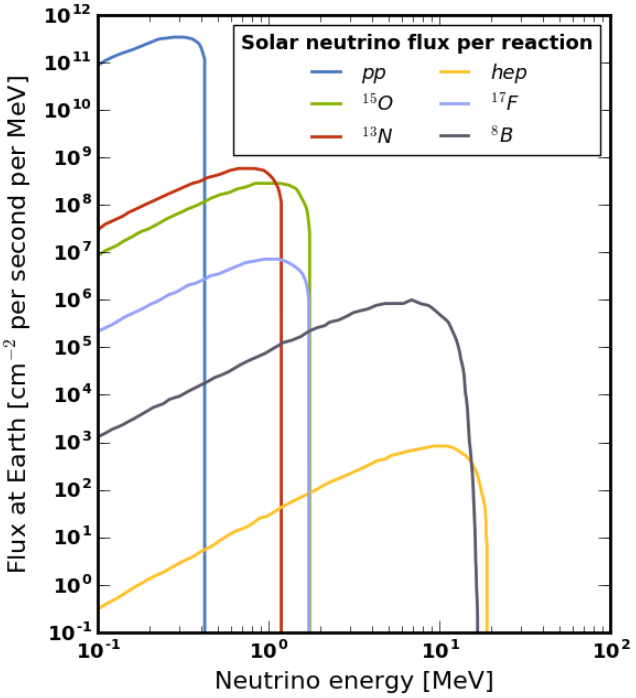

FIG. 7: Theoretical Solar Neutrinos Fluxes for all processes. We are interested in the MeV range and will therefore only take into account the B^8 and hep processes.

The fluxes for these processes are averaged and listed in table . The figures and fluxes were extracted from Bahcall, et al. [9]. As we can see, the hep flux is about 3 orders of magnitude smaller than ^8B flux, therefore it will also be ignored.

Process	Flux (cm^{-2}s^{-1})
$^8B \rightarrow {}^8Be^* + e^+ + \nu^e$	5.05 x 10^6
$^3He + \mathrm{p} \rightarrow {}^4He + e^+ + \nu^e$	9.3 x 10^3

I inject the neutrinos into the medium using my neutrino-injector tool. The neutrino injector tool was first introduced in section but was created for injection electron anti-neutrinos from the reactor core. Here it is simply re-purposed by applying a different flux and a different incoming direction. However, the liquid scintillator does not take into account angular properties of the neutrinos, therefore the only thing that is changed is the flux and energy distributions. My distribution of the fluxes as a function of neutrino energy is shown in figure 8. These fluxes were initially measured by the SNO experiment for only electron neutrino interactions and was found to be $\Phi = 1.76\mathrm{X}10^6 \mathrm{cm}^{-2}\mathrm{s}^{-1}$. The result is consistent with my averages shown in when divided by the number of neutrino flavors. Since the flux was presented as an average flux over the entire ^8B process, I have simulated the energy for these neutrinos using a uniform random number generator. When summing over the entire energy range, we must taken into account the number of simulated events. It is also clear from the figure, that the solar neutrino flux does not care about any distance or depths, therefore it is considered an irreducible background. This means that nothing can ever be done to minimize our impact from this background (unless we extinguish the sun!).

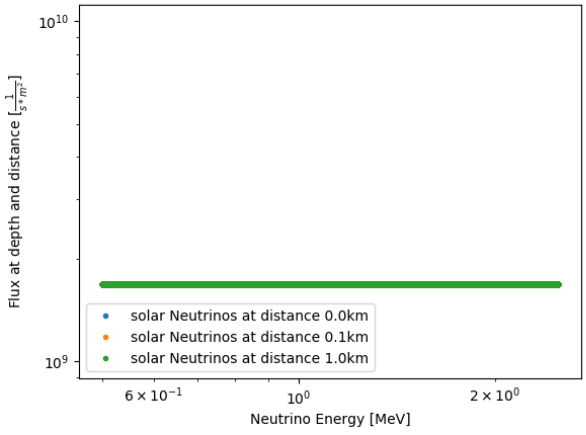

FIG. 8: Solar neutrino fluxes for electron anti-neutrinos. The average measured neutrino flux extracted from the SNO+ experiment [7] and re-weighted to the energy ranges we are interested in. Due to the small flux, I assume a uniform distribution of the fluxes as a function of energy.

RESULTS

Given the reactor neutrino fluxes shown in section, the solar neutrino fluxes from section , and atmospheric muon fluxes in section , we can begin to compute optimal depths. For a particular depth, the muons are multiplied by the effective area of our detector assuming all muons interact as soon as they come into contact with the liquid scintillator. For a particular distance from the reactor, the neutrino flux is multiplied by the cross section formula in eq 3, this gives us the number of interactions per second per nucleon. At this point it is simply multiplied by the number of nucleons inside the effective volume in the detector. This is repeated for both reactor and solar neutrinos. This gives us the number of observed inverse beta decay interactions per second. The rates are then integrated over a time window of 1s and the observed significance is computed. This significance is then computed for several depths, the results of several of these measurements are shown in figure 9. The uncertainty in the measurement is due to the error in the calculation of muon fluxes and was shown in figure: 5 to affect the lowest energy muons, which also have the largest weights.

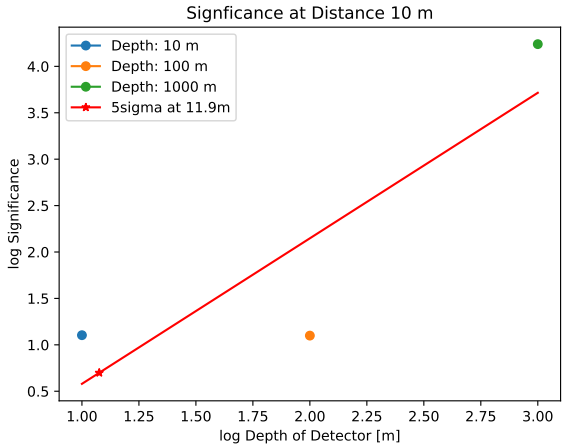

FIG. 9: The significance for the baseline experiment of placing a detector 10m away from a nuclear reactor core. The three points indicate the different depths inside granite and the red line shows a fit to the points. A 5sigma observation is required and shown with the star marker to be 11.9m depth.

The three dots in figure 9 show the computed significance for eq 5. The values differ because they are different approximations made for either large signals or backgrounds. For a detector placed 10m away from a reactor core, the optimal depth to place a detector would be 11.9m under granite, basically at surface. It is important to keep in mind that the reason for this high significance at the Earth's surface is because the detector used is of high density and perfect efficiency is assumed.

This technique is repeated for several distance from the reactor core and shown in .

For a reactor experiment placed 1km away from the source, we would need to place the detector over 4km under granite stone. To put this into perspective the LZ dark matter experiment is located at 4850L in the Sanford Underground Research Facility[18], this facility is located 4850 feet underground which translates to 1.5km. It is therefore important to place the detectors close to the nuclear reactor is attempting to observe a significance signal of reactor neutrinos.

CONCLUSION AND OUTLOOK

The major assumptions made for these studies is that the muons will always trigger the detector and therefore it must be placed at a size able depth such that this "noise" does not saturate our detector. The second assumption made is that the atmospheric muons and solar neutrinos are both incoming at zenith angles of $\theta = 0$. In reality, these muons and neutrinos have angular as well as temporal dependence (solar cycles, weather on surface, etc...). These studies show the optimal placement of a detector inside a mine surrounded of granite stone.

In a real world application, the distance would be defined by the interesting physics one wishes to measure (perhaps neutrino oscillations) or an attempt to be covert (monitoring needs to be hidden). In the real world application, the material surrounding the neutrino detector would also need to be measured such that the correct energy loss curves for the muons can be constructed. Given sufficient time to calibrate the detector, it would also be recommended to add a single layer (or two) of some sort of Geiger counter on the top and sides of the detector. The Geiger counter would indicate the presence of an incoming muon and therefore prevent the detector from becoming saturated with this background. It would also be possible to use the delayed photon energy and time from the neutron capture to apply a cut and further reduce the presence of muon backgrounds. All of these studies are left for a later date.

CODE

The project and all corresponding data has been uploaded to git-hub in the following url `https://github.com/manuel92780/reactor_neutrino_project`. All code for simulating individual events was created by me. All calculations were performed in the code framework. To run your own calculation, run the following commands:

```
source generate_muons.sh
source generate_neutrinos.sh
```

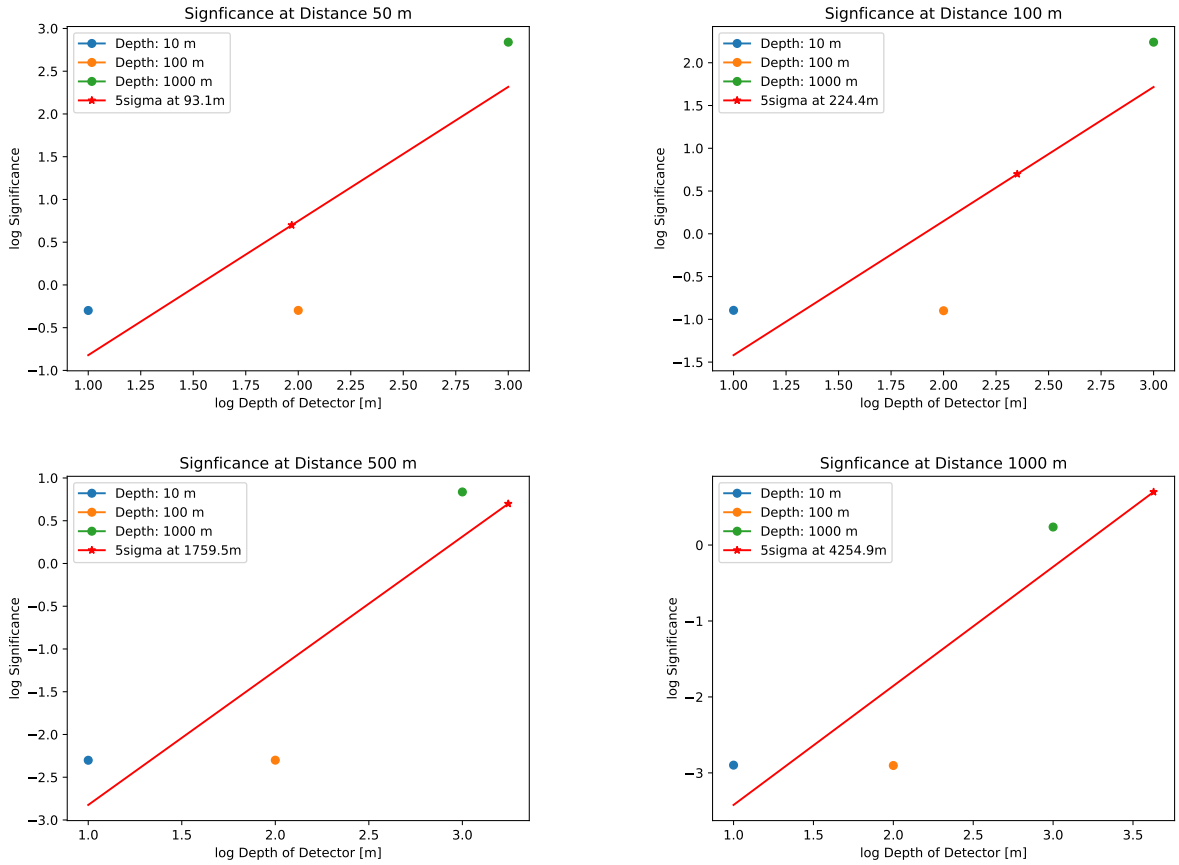

FIG. 10: The experiment is repeated for various distances from the source. For distances above 500m, the required depth of the detector would be over 2km. This approaches the depth of the LZ experiment in North Dakota and should be taken as an extreme case. These show that experiments that attempt to measure electron anti-neutrinos from a nuclear reactor should be placed within 500m of the source.

`python compute_sig.py -dist 10`

. The code will internally run the procedure and extract the best depth for a detector placed 10m away from the reactor core. The "10" can be modified for any distance at will. The "fluxes.py" file contains the propagation of muons to particular depth and the "bethe_bloche.py" contains the calculation of the energy losses at particular energies. "bethe_bloche.py" would need to be modified to accommodate the parameters of the material in which the muons would be propagated through. "compute_sig.py " contains the parameters for the detector configuration and can also be modified to accommodate any detector of your choice.

[1] C. L Cowan Jr.; F. Reines; F. B. Harrison; H. W. Kruse; A. D McGuire (July 20, 1956). "Detection of the Free Neutrino: a Confirmation". Science. 124 (3212): 1034.

[2] Daya Bay Proposal – "A Precision Measurement of the Neutrino Mixing Angle 13 Using Reactor Antineutrinos at Daya Bay", Daya Bay Collaboration, Dec. 2006, arXiv:hep-ex/0701029

[3] M. Yeh, A. Garnov, R.L. Hahn, Nuclear Instruments and Methods in Physics Research A 578 (2007) 329.

[4] https://www.eia.gov/nuclear/state/archive/2010/newyork/

[5] M. Tanabashi et al. (Particle Data Group), Phys. Rev. D 98, 030001 (2018).

[6] Tavernier, S. Experimental Techniques in Nuclear and Particle Physics, isbn=9783642008290, 2010, Springer Berlin Heidelberg.

[7] Chen, M. (2005). "The SNO Liquid Scintillator Project". Nuclear Physics B - Proceedings Supplements. 154: 6566.

[8] "Rock Types and Specific Gravities". EduMine. Retrieved 2017-08-27.

[9] J. N. Bahcall, A. M. Serenelli, and S. Basu, Astrophys. J. 621, L85 (2005), astroph/0412440.

[10] Y. Fukuda et al. [Super-Kamiokande Collaboration], Phys. Lett. B 433, 9 (1998) [arXiv:hep-ex/9803006]

[11] Halzen, Francis, and Alan Douglas. Martin. Quarks and Leptons: an Introductory Course in Modern Particle Physics. John Wiley, 2016.

[12] M.Honda, T.Kajita, S.Midorikawa, K.Kasahara. "Calculation of the Flux of Atmospheric Neutrinos". Phys.Rev.

D52 (1995) 4985-5005
[13] T K Gaisser 2006 J. Phys.: Conf. Ser. 47 15.
[14] D. Heck, J. Knapp, J.N. Capdevielle, G. Schatz, T. Thouw . "CORSIKA: A Monte Carlo Code to Simulate Extensive Air Showers". https://www.ikp.kit.edu/corsika/index.php .
[15] E.V. Bugaev, A.Misaki, V.A.Naumov, T.S. Sinegovskaya, S.I. Sinegovsky, N.Takahashi. "Atmospheric muon flux at sea level, underground, and underwater". Phys. Rev. D58 054001 (1998).
[16] R. R. G. Marleau, A. Hebert, and R. Roy, A User Guide for DRAGON, Report IGE-236 Rev. 1 (2001).
[17] S.I.Bityukov and N.V.Krasnikov, The Search for New Physics by the Measurement of the Four-jet Cross Section at LHC and TEVATRON, Modern Physics Letter A12(1997)2011, also hep-ph/9705338.
[18] "Sanford Underground Research Facility Overview — Sanford Underground Research Facility". www.sanfordlab.org. Retrieved 2019-04-26.